

Entanglement-assisted variational algorithm for discrete optimization problems

Lorenzo Fioroni^{1,2,*} and Vincenzo Savona^{1,2,†}

¹Laboratory of Theoretical Physics of Nanosystems,
École Polytechnique Fédérale de Lausanne (EPFL), CH-1015 Lausanne, Switzerland

²Center for Quantum Science and Engineering,
École Polytechnique Fédérale de Lausanne (EPFL), CH-1015 Lausanne, Switzerland

From fundamental sciences to economics and industry, discrete optimization problems are ubiquitous. Yet, their complexity often renders exact solutions intractable, necessitating the use of approximate methods. Heuristics inspired by classical physics have long played a central role in this domain. More recently, quantum annealing has emerged as a promising alternative, with hardware implementations realized on both analog and digital quantum devices. Here, we develop a heuristic inspired by quantum annealing, using Generalized Coherent States as a parameterized variational Ansatz to represent the quantum state. This framework allows for the analytical computation of energy and gradients with low-degree polynomial complexity, enabling the study of large problems with thousands of spins. Concurrently, these states capture non-trivial entanglement, crucial for the effectiveness of quantum annealing. We benchmark the heuristic on the three-dimensional Edwards-Anderson model and compare the solution quality and runtime of our method to other popular heuristics. Our findings suggest that it offers a scalable way to leverage quantum effects for complex optimization problems, potentially surpassing conventional alternatives in large-scale applications.

I. INTRODUCTION

Optimization problems play a pivotal role in a wide range of fields. From optimizing the allocation of medical resources in healthcare systems [1, 2] to improving energy distribution in smart grids [3, 4] and enhancing traffic flow in urban areas [5, 6], these tasks aim to identify which input from a pre-defined set minimizes a given metric, referred to as the *loss function*. A paradigmatic class of optimization problems is that of *Quadratic Unconstrained Binary Optimization* (QUBO) [7], where the loss function is a quadratic form of binary variables. Despite their simple formulation, QUBO problems are known to be computationally challenging, as they belong to the NP-Hard complexity class [8, 9]. This means that no algorithm is known to solve an arbitrary QUBO instance in polynomial time, and the required computational resources grow exponentially with the problem size. At the same time, QUBO problems are of great practical relevance, as any other NP problem can be efficiently reduced to them [10]. Consequently, the development of fast algorithms for approximating the optimal solution of these problems is of great interest. These can be broadly divided into two categories: *approximation algorithms* and *heuristics*. Approximation algorithms aim to find a solution that is guaranteed to be up to a certain factor off the optimal one [11, 12], while heuristics aim to find a good solution in a reasonable amount of time, without any guarantee of optimality [13].

Multiple heuristics have been developed to tackle QUBO problems efficiently, often inspired by various areas of physics [14–19]. For example, simulated anneal-

ing [20] emulates the behavior of a system at finite temperature, exploring the configuration space via thermal fluctuations, while simulated bifurcation [21] draws inspiration from nonlinear dynamics to navigate the solution landscape efficiently. These physics-inspired heuristics have further motivated the development of specialized hardware accelerators, such as the Coherent Ising Machine [22] and the Fujitsu Digital Annealer [23–25], among others.

Quantum physics offers a promising approach to solving QUBO problems through *quantum annealing* [26–30]. In quantum annealing, the classical problem is first mapped onto the ground state of a quantum Hamiltonian, which is then obtained via adiabatic state preparation. Despite being the subject of extensive research, a definitive demonstration of the advantage of quantum annealing over classical heuristics remains an open question. Numerous studies have been conducted, aimed at simulating its underlying physical process to understand the effects of finite temperature, noise, diabatic transitions, and other deviations from the ideal scenario [31–33]. The goal of these studies is to describe the quantum state and its dynamics as accurately as possible, to ultimately characterize quantum annealing and identify its differences from classical optimization methods. To this purpose, a variety of techniques have been adopted, mostly relying either on Path Integral Monte Carlo (PIMC) [34–36], or on Variational Monte Carlo (VMC) dynamics. In the latter case, several advanced variational Ansätze have been used to capture the many-body quantum correlations arising along the evolution [37, 38]. While these studies are crucial for understanding the mechanisms of quantum annealing, they are not suitable for use as efficient optimization heuristics due to their high computational demands and unfavorable scaling with problem size. Additionally, many of these methods rely on Monte

* lorenzo.fioroni@epfl.ch

† vincenzo.savona@epfl.ch

Carlo sampling, which further increases computational overhead. In contrast, a classical optimization algorithm inspired by quantum annealing might forgo some physical accuracy in favor of greater efficiency. Recent studies in this direction proposed using a product-state Ansatz to describe the state of the system [39, 40]. This method, referred to as Local Quantum Annealing (LQA), allows simulating the state's evolution analytically, avoiding the need for Monte Carlo sampling. However, the simplicity of the Ansatz severely limits the range of states it can represent, resulting in a fast but less accurate heuristic. In particular, it cannot capture any of the entangled states that arise during quantum annealing.

In this work, we propose a quantum-inspired heuristic for solving QUBO problems. Drawing inspiration from the quantum annealing process, we develop an efficient variational procedure that emulates its dynamics in a fully analytical way. The variational Ansatz we employ is based on Generalized Group-Theoretic Coherent States (GCS) [41, 42], which allow for the efficient evaluation of the energy and its gradient. At the same time, it captures to some extent the entanglement structure that emerges during the quantum annealing process, thus leveraging the advantage it provides. Without the need for Monte Carlo sampling, our algorithm is highly scalable and allows for the efficient optimization of problems with thousands of variables.

We benchmark our algorithm on random instances of the three-dimensional Edwards-Anderson model [8], comparing its performance to that of standard heuristics such as Simulated Annealing (SA) [20], Local Quantum Annealing (LQA) [39], and Parallel Tempering with Isoenergetic Cluster Moves (PT-ICM) [43]. We identify parameter regimes where our algorithm holds an advantage over the other methods tested, and provide evidence that for large system sizes it outperforms them all.

II. RESULTS

A QUBO problem is fully specified by a real-valued and symmetric matrix J and a real-valued bias vector \mathbf{b} through the relation

$$\mathbf{z}^* = \operatorname{argmin}_{\mathbf{z} \in \{0, 1\}^N} \left[\sum_{i,j=1}^N J_{ij} z_i z_j + \sum_{i=1}^N b_i z_i \right], \quad (1)$$

which also defines its solution \mathbf{z}^* . Up to a linear transformation of its variables, the binary optimization problem in Eq. (1) can be mapped onto

$$\mathbf{s}^* = \operatorname{argmin}_{\mathbf{s} \in \{\pm 1\}^N} \left[\sum_{i,j=1}^N W_{ij} s_i s_j + \sum_{i=1}^N c_i s_i \right], \quad (2)$$

where $W_{ij} = J_{ij}/4$ and $c_i = (b_i + \sum_j J_{ij})/2$. In the following, we will consider QUBO problems expressed as in Eq. (2). Without loss of generality, we will omit the

bias term \mathbf{c} , as it can be accounted for in the quadratic term W at the cost of introducing an additional variable with fixed value $s_{N+1} = 1$.

A. Quantum annealing

The solution of optimization problems using quantum annealing involves mapping the problem onto the ground state of a quantum Hamiltonian, which is then adiabatically prepared [44, 45]. In case of the QUBO problem in Eq. (2), the associated quantum Hamiltonian is that of a spin- $1/2$ system with Ising interactions

$$\hat{\mathcal{H}}_I = \sum_{i,j=1}^N W_{ij} \hat{\sigma}_z^{(i)} \hat{\sigma}_z^{(j)}, \quad (3)$$

where $\hat{\sigma}_z^{(i)}$ is the Pauli-Z operator acting on the i -th spin.

The adiabatic state preparation procedure begins by initializing the system in the ground state of a simple Hamiltonian, typically chosen so that its ground state is known analytically, and then continuously transforms it into $\hat{\mathcal{H}}_I$ over time. According to the adiabatic theorem, if this transformation occurs sufficiently slowly, the system will remain in the instantaneous ground state of the time-dependent Hamiltonian throughout the evolution [46]. More precisely, we can set $|\psi_0\rangle = |+\rangle^{\otimes N}$ as the initial state at time $t = 0$ and implement the time-dependent Hamiltonian

$$\hat{\mathcal{H}}(t) = \frac{t}{T} \hat{\mathcal{H}}_I + \left(1 - \frac{t}{T}\right) \hat{\mathcal{H}}_{\text{TF}}, \quad (4)$$

where $\hat{\mathcal{H}}_{\text{TF}} = -\sum_i \hat{\sigma}_x^{(i)}$ is the transverse field Hamiltonian. At the beginning of the annealing schedule, i.e. at time $t = 0$, the state $|\psi_0\rangle$ is the ground state of the initial Hamiltonian $\hat{\mathcal{H}}_{\text{TF}}$. The system then undergoes adiabatic time evolution, gradually transforming toward the ground state of $\hat{\mathcal{H}}_I$ as the annealing process reaches the final time $t = T$. In the limit of large annealing times T , the adiabatic theorem ensures that the system remains in the instantaneous ground state of the Hamiltonian throughout the entire process. The choice of T is therefore crucial for the success of the adiabatic algorithm and should be related to the minimal energy gap Δ_{\min} between the ground state and the first excited state of the Hamiltonian during the evolution. Specifically, T should be chosen such that $T \gg 1/\Delta_{\min}^2$ to satisfy the adiabatic condition and minimize the probability of diabatic transitions that could lead the system out of the ground state [44, 45]. The final state after the evolution is by construction a product state encoding the solution to the original optimization problem. This can be read out by measuring the individual spins in the computational basis.

While quantum annealing is a promising approach to solving optimization problems, the extent of its advantage over classical algorithms remains under active debate [29, 34, 43, 47–49]. Yet, the general agreement

is that the potential advantage offered by quantum annealing is intrinsically linked to the formation of entanglement during the evolution according to the time-dependent Hamiltonian [43, 50–52].

B. Simulated quantum annealing

Studies simulating quantum annealing on a classical computer typically rely on techniques such as PIMC or VMC to describe the quantum system [34–38], as their expressive power allows for the accurate representation of the physical state. Here, we approach quantum annealing from a different perspective. We do not seek to simulate the quantum state and its dynamics accurately, but rather to develop a heuristic optimization algorithm that takes inspiration from the quantum annealing process, while being computationally efficient and scalable to large problem sizes. Key to this approach is the choice of an Ansatz that partially trades physical accuracy for computational efficiency, in particular by avoiding the need for Monte Carlo sampling. Taking this idea to its logical extreme, recent studies [39, 40] proposed approximating the state along the annealing schedule via an Ansatz of product, and thus not entangled, states in the form

$$|\psi(\boldsymbol{\theta})\rangle = |\theta_1\rangle \otimes |\theta_2\rangle \otimes \dots \otimes |\theta_N\rangle, \quad (5)$$

where each $|\theta_i\rangle$ is a single-spin state fully specified by a real parameter θ_i . This method, referred to as *Local Quantum Annealing* (LQA), has the advantage that both the expectation value of the energy along the annealing schedule, and its gradient with respect to the parameters $\boldsymbol{\theta}$, can be computed analytically, without requiring Monte Carlo sampling. On the other hand, the Ansatz in Eq. (5) cannot capture any entanglement between the spins, thus missing the feature believed to be at the core of the quantum annealing’s potential advantage.

C. Generalized Atomic Coherent States

The spin- $1/2$ product states used by LQA are a subset of the larger class of *Group-Theoretic Coherent States* [53, 54]. These states allow for the efficient analytical evaluation of expectation values of Pauli operators and their gradient vectors [41], but they are limited to the description of unentangled states only.

On the other hand, the ability to efficiently compute expectation values analytically is not exclusive to the product states in Eq. (5). Specifically, the class of *Generalized Group-Theoretic Coherent States* has been recently shown to extend that of Group-Theoretic Coherent States by introducing non-trivial correlations between the system’s components, while still allowing for a computationally efficient evaluation of the energy and its gradient [41, 42]. In the following, we will extensively refer to the Generalized Group-Theoretic Coherent

States built upon the SU(2) group for spin- $1/2$ particles as *GCS states*. A GCS state is defined via the relation $|\psi(x, M, y)\rangle = \mathcal{U}(y)\mathcal{V}(M)\mathcal{U}(x)|+\rangle^{\otimes N}$, where the operators \mathcal{U} and \mathcal{V} can be expressed as

$$\mathcal{U}(x) = \bigotimes_{j=1}^N \exp\left(-i \sum_{k \in \{x,y,z\}} x_{jk} \hat{\sigma}_k^{(j)}\right), \quad (6)$$

$$\mathcal{V}(M) = \exp\left(-i \sum_{j \neq k} M_{jk} \hat{\sigma}_z^{(j)} \hat{\sigma}_z^{(k)}\right). \quad (7)$$

Here, the variational parameters are all real-valued and are grouped into two $N \times 3$ matrices, x and y , and a symmetric $N \times N$ coupling matrix M . The total number of parameters is therefore $N_{\text{par}} = 6N + N(N-1)/2$. Importantly, since $\mathcal{V}(M \equiv 0) = \mathbb{I}$ and any two product states are related by factorized rotations, all product states can be represented exactly by this Ansatz. Furthermore, the two-body operators in $\mathcal{V}(M)$ introduce correlations between the spins, generating non-Gaussian entanglement within the system.

The optimization scheme we developed initializes the system in a GCS state approximating $|\psi_0\rangle = |+\rangle^{\otimes N}$, with $y \equiv 0$ and $M \equiv 0$. Then, the Hamiltonian is varied according to the annealing schedule, evaluating Eq. (4) over a discrete grid of N_t times such that

$$t_j < t_{j+1} \forall j = 1 \dots N_t, \quad t_1 = 0 \text{ and } t_{N_t} = T. \quad (8)$$

The loss function is defined to be the expectation value of the time-dependent Hamiltonian

$$\mathcal{L}_{t_j}(x, M, y) = \langle \psi(x, M, y) | \hat{\mathcal{H}}(t_j) | \psi(x, M, y) \rangle, \quad (9)$$

and it is minimized at each time step t_j by the variational algorithm, updating the parameters via gradient-based optimization similarly to Refs. [39, 40]. We remark that this protocol differs from the unitary dynamics that characterizes the physical quantum annealing process and, from empirical evidence, is more effective in approaching the global minimum when diabatic effects start being relevant. Moreover, under the assumption

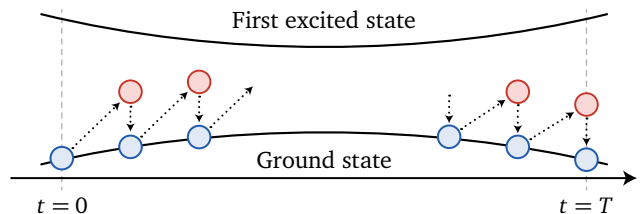


FIG. 1: Sketch of the optimization scheme. As the Hamiltonian evolves, the parameters of the Ansatz are updated to minimize the expectation value of the Hamiltonian. Each time step, only one single update is performed.

that the adiabatic evolution results in the state remaining close to the instantaneous ground state along the annealing schedule, we simplify the algorithm by executing only one gradient-based update of the parameters at each time step, as sketched in Fig. 1. The updates are performed by employing the ADAM optimizer [55]. The result is a highly efficient optimization algorithm that allows us to study problems of thousands of variables with ease. Specifically, as we show in Sec. IV, GCS states allow for the analytical evaluation of expectation values of Pauli operators at a computational cost scaling as $\mathcal{O}(N)$. The number of operations required to evaluate the expectation value of the Hamiltonian, thus, depends on the number of non-zero elements in the adjacency matrix W . For dense matrices or analogous problems with all-to-all connections, $\mathcal{O}(N^2)$ expectation values need to be computed. The total complexity of the algorithm is therefore $\mathcal{O}(N^3)$. As the matrix W becomes sparser, on the other hand, the complexity of the algorithm improves. In particular, for a sparse matrix W containing $\mathcal{O}(N)$ nonzero elements, the computational cost is reduced to $\mathcal{O}(N^2)$, as shown in Fig. 2.

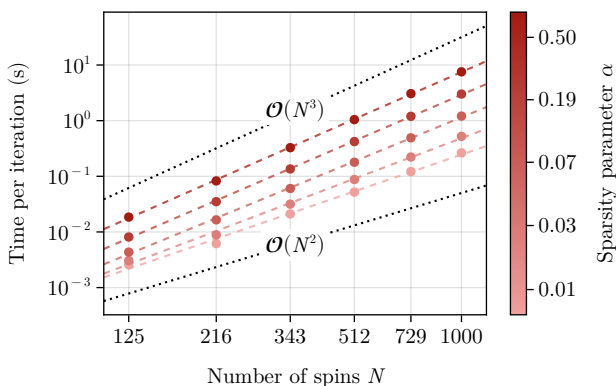


FIG. 2: Time per iteration as a function of the non-zero elements in the adjacency matrix W . The number of non-zero elements is varied according to $N_{\text{nnz}} = (1 + \alpha(N - 1))N$. As the number of non-zero elements is decreased, the execution time per iteration crosses over from $\mathcal{O}(N^3)$ to $\mathcal{O}(N^2)$ scaling. The two dotted lines represent guides to the eye for the two scaling regimes.

At the end of the annealing schedule, a classical solution to the optimization problem is obtained by evaluating the expectation value $z_j = \langle \hat{\sigma}_z^{(j)} \rangle$ on each spin and rounding it to the closest integer between -1 and 1 . Note that while the ground state of \hat{H}_I is by construction a classical state, the approximate nature of the algorithm and the finite annealing time T inevitably lead to a final state with some residual quantum superposition of classical states. In these cases, the simple protocol to extract a classical solution may lead to discretization errors, and thus represents an additional source of approximation for the optimization algorithm. These errors can be mitigated by employing more refined discretization tech-

niques [56, 57], but in the benchmarks presented in this work, we didn't notice a significant improvement from these methods compared to the basic rounding protocol.

D. Benchmark

We test the performance of our algorithm on a set of random instances of the three-dimensional Edwards-Anderson model [8]. Due to the cubic topology of the lattice, the adjacency matrix W is sparse and the number of expectation values to be evaluated scales as $\mathcal{O}(N)$, resulting in an overall $\mathcal{O}(N^2)$ scaling of the algorithm's complexity. We assess the quality of the solutions by comparing their energies with those from LQA [39], a standard Simulated Annealing (SA) implementation [20], and a highly-optimized Parallel Tempering algorithm with Isoenergetic Cluster Moves (PT-ICM) [43]. For each instance, we find the global minimal energies E_0 using the Gurobi [58] exact solver and evaluate the performance based on the relative error $\varepsilon = (E - E_0)/|E_0|$. Because of the exponential scaling of Gurobi's runtime, the problem sizes studied in this section are limited to 2197 spins, corresponding to a cubic lattice with 13 spins per side.

Fig. 3 shows the evolution of the relative error ε as a function of the number of spins N . In this comparison, the algorithms are run on 1000 random instances for $N_t = 1000$ iterations, and the median of ε is reported. The shaded regions represent the interquartile range of the resulting distributions, defined as the range between the 25% and the 75% of the distribution, thus covering the middle 50% of the data. We observe that, while SA and LQA achieve comparable error rates, our algorithm consistently outperforms them by a significant margin. When comparing it to PT-ICM, on the other hand, we find that for small system sizes the latter returns lower-

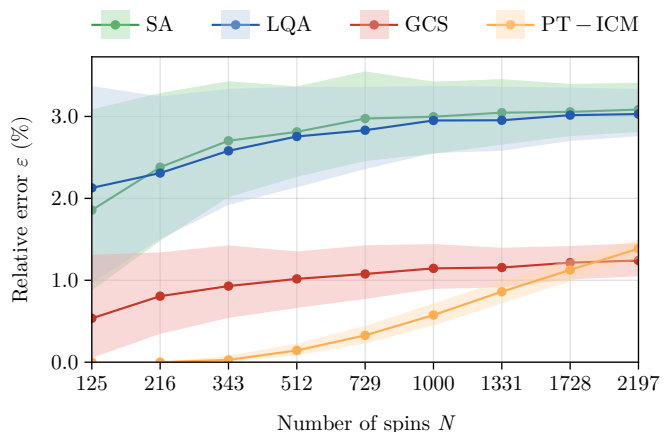


FIG. 3: Median relative error ε as a function of the number of spins N . Each method is run for $N_t = 1000$ iterations on 1000 random problem instances. The shaded regions represent the interquartile ranges of the resulting distributions.

energy solutions on average. However, as the number of spins increases, the performance of PT-ICM quickly deteriorates, while GCS displays a more gradual increase in the relative error. For the largest system sizes considered, GCS outperforms all other methods tested.

In Tab. 1 we present the execution times for the four heuristics under comparison, alongside those of the Gurobi solver. We emphasize that both PT-ICM and Gurobi are highly optimized algorithms, whereas our self-implemented versions of SA, LQA and GCS, despite being carefully developed, may benefit from further optimization. Therefore, we argue that execution times provide only partial insight into the relative performance of the heuristics. A more informative comparison correlates the algorithms' results to the number of iterations N_t they have been executed for, while accounting for the distinct complexity scaling of each heuristic.

N	Runtime (s)				
	SA	LQA	GCS	PT-ICM	Gurobi
125	0.03	0.01	2.73	0.19	0.10 (0.09, 0.13)
216	0.03	0.02	7.12	0.33	0.62 (0.46, 0.93)
343	0.04	0.03	20.33	0.53	2.91 (2.61, 3.22)
512	0.07	0.04	44.02	0.79	8.67 (7.25, 10.06)
729	0.09	0.05	88.84	1.12	25.55 (22.54, 29.26)
1000	0.13	0.07	167.49	1.54	70.53 (58.08, 89.57)
1331	0.18	0.13	306.17	2.04	157.50 (127.34, 251.59)
1728	0.23	0.15	520.48	2.64	664.59 (423.89, 1353.82)
2197	0.31	0.18	880.10	3.36	1568.23 (934.55, 3125.83)

TABLE 1: Median runtimes of the tested algorithms as a function of the number of spins N . Runtimes of SA, LQA, GCS and PT-ICM instances showed negligible variance. Gurobi's runtime instead highly depends on the problem instance, resulting in a broad and skewed distribution. In this case, we reported within brackets the 25th and 75th percentiles in addition to the median.

As reported in Tab. 1, it is important to acknowledge that one single iteration of GCS is computationally more expensive than one iteration of PT-ICM. As all heuristics perform better when the number of iterations is increased, a fair comparison should account for this difference by adjusting N_t for each method accordingly. In Fig. 4a, we present the relative error ε as a function of the number of iterations N_t , for different system sizes, providing a complementary evaluation of the algorithms' performance. As expected for simulated classical annealing methods, the relative error of SA and PT-ICM decreases steadily with N_t . In contrast, GCS asymptotically approaches a constant value. We argue that this constant value is due to the limited expressivity of the Ansatz. The similarity of LQA's trend to GCS supports this hypothesis, with LQA converging to a higher error level due to the absence of entanglement in the product state Ansatz. The fast convergence of GCS allows us to identify a range of annealing times T where our

algorithm outperforms all other methods tested. This region, highlighted in Fig. 4a, expands as the system size increases. Since the computational cost of GCS scales quadratically with system size, whereas PT-ICM scales linearly, it is crucial to analyze how the advantage region expands with the number of spins to assess the relative performance of these algorithms. This analysis is presented in Fig. 4b, where the length of the advantage region is plotted against the number of spins. A fit to the data reveals that the advantage region scales linearly with the number of spins. Hence, to obtain an advantage with PT-ICM in the limit of large systems, a number of iterations larger by a factor $\mathcal{O}(N)$ than GCS is needed, suggesting that in this limit the complexity of both algorithms scales with $\mathcal{O}(N^2)$ to reach a given relative error.

The results presented in Figs. 3 and 4a collectively demonstrate that, for fixed annealing times and in the limit of large system sizes, the GCS algorithm outperforms all other methods tested in this study. This advantage persists even when the number of iterations is not fixed, provided that an error level above the asymptotic limit achieved by GCS is acceptable. In such scenarios, GCS requires significantly fewer iterations to reach the specified error level compared to PT-ICM. Consequently, for large problem sizes, GCS may represent a valid alternative to classical annealing methods, with a significantly lower relative error already at moderate number of iterations.

III. DISCUSSION

In this work, we introduced a novel quantum-inspired heuristic for solving QUBO problems. We developed a variational procedure inspired by the quantum annealing process, for which the loss function and its gradient can be computed analytically, allowing for the optimization of problems with thousands of variables within minutes. The variational Ansatz, based on Generalized Group-Theoretic Coherent States, partially captures the entanglement emerging during the quantum annealing dynamics, leading to an approximate solution outperforming a corresponding uncorrelated Ansatz. Concurrently, the analytical evaluation of the expectation values of the Hamiltonian and its gradient allows for a highly scalable algorithm with a low-degree polynomial complexity in the number of spins.

We demonstrate the effectiveness of our algorithm on the 3D Edward-Anderson model, through comprehensive benchmarking against established optimization methods. Our results clearly identify a wide range of cases where GCS outperforms all other methods tested in terms of the quality of the solutions found, including the Parallel Tempering algorithm with Iso-energetic Cluster Moves. In particular, we show that for a fixed number of iterations and in the limit of large system size, the GCS algorithm shows the best performance. Moreover, we identify a threshold in relative error, above which our algorithm

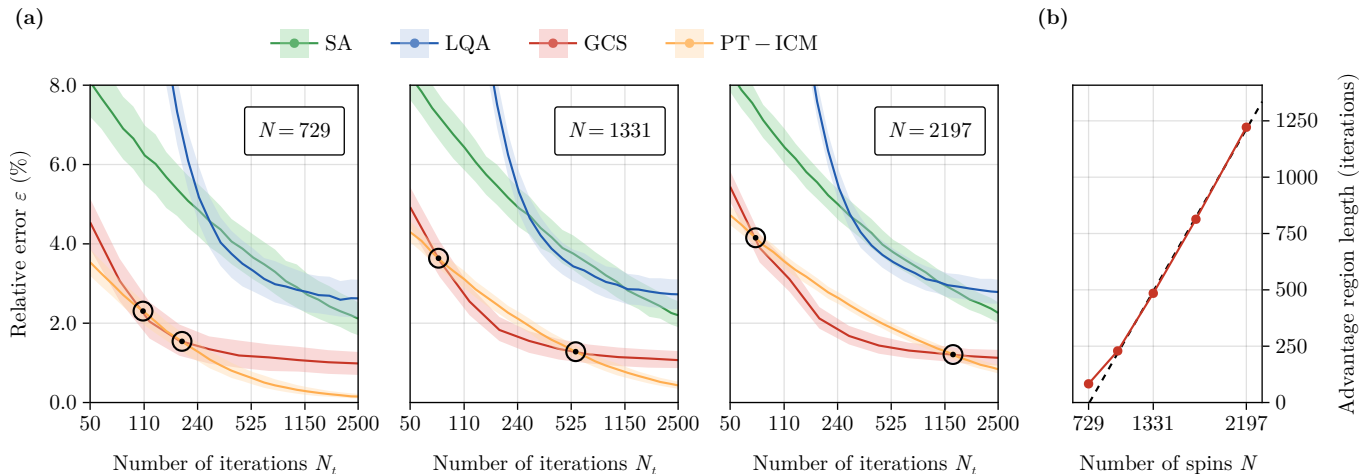


FIG. 4: **(a)** – Median relative error ε as a function of the number of iterations N_t . Each method is benchmarked on 1000 random problems. The shaded regions represent the interquartile range of the resulting distributions. We identify an expanding region in the parameter space, delimited by black dots, where GCS outperforms PT-ICM. **(b)** – Length of the advantage region as a function of the number of spins. The black, dashed line represents a linear fit to the data.

outperforms all other methods in terms of the required number of iterations. In this regime, the rapid convergence of GCS allows us to reach low error levels with fewer iterations.

Several avenues for further research remain open. Increasing the Ansatz’s expressivity, for example, could potentially lead to a more accurate representation of the quantum annealing dynamics, thus improving the quality of the solutions. This could be achieved by employing linear superpositions of GCS states. Indeed, if the states in the superposition share the same values of the y and M parameters, differing only in the x parameters, the Ansatz preserves the possibility to compute the loss function and its gradient analytically.

In the opposite direction, one could consider simplifying the Ansatz by enforcing structures on the parameters, thus reducing their number and the complexity of the optimization problem. A prototypical case would be the invariance of the problem under specific symmetries, which could be readily incorporated into the Ansatz, eventually accelerating its optimization procedure. In the case of problems with a known topology, like the one studied here, one could also consider a sparse matrix M bearing the same structure as the adjacency matrix W . This would reduce the expressivity of the Ansatz, but still incorporate entanglement while considerably speeding up the optimization algorithm compared to the GCS with an arbitrary parameter matrix M .

In conclusion, the results presented in this work demonstrate the potential of quantum-inspired heuristics for solving large-scale optimization problems. Our comparison against simpler Ansätze shows that the entanglement captured by the GCS framework plays a crucial role

in improving the quality of the solutions. Our work thus paves the way for leveraging quantum effects for complex classical optimization problems, potentially opening new avenues for the development of efficient algorithms for large-scale optimization tasks.

IV. METHODS

At the core of our algorithm’s efficiency lies the analytical evaluation of both the expectation value of the Hamiltonian and its gradient. In this section, we provide a concise overview of the method employed to evaluate the loss function. For a more comprehensive explanation, as well as a similar treatment of the gradient, we direct the reader to the Supplementary Information.

We begin by noting that the loss function in Eq. (9) is expressed as a linear combination of 1- and 2-local terms in the form of $\langle \hat{\sigma}_x^{(i)} \rangle$ and $\langle \hat{\sigma}_z^{(i)} \hat{\sigma}_z^{(j)} \rangle$, respectively. Here, we detail the procedure used to estimate $\langle \hat{\sigma}_x^{(i)} \rangle$ for a specific spin index i . The evaluation of $\langle \hat{\sigma}_z^{(i)} \hat{\sigma}_z^{(j)} \rangle$ follows an analogous approach, leading to similar results.

Let us introduce the notation $\hat{\sigma}_\alpha^{(i)}$ (using a Greek index) to represent the Pauli operators σ_- , σ_z and σ_+ for $\alpha \in \{-1, 0, 1\}$, respectively. Additionally, we define the states

$$|\psi(x)\rangle = \mathcal{U}(x) |+\rangle^{\otimes N}, \quad (10)$$

$$|\psi(x, M)\rangle = \mathcal{V}(M)\mathcal{U}(x) |+\rangle^{\otimes N} \quad (11)$$

to simplify our notation. The operator $\mathcal{V}(M)$ obeys the

following relation, reported in Guaita *et al.* [41]:

$$\mathcal{V}(M)^\dagger \hat{\sigma}_\alpha^{(i)} \mathcal{V}(M) = \hat{\sigma}_\alpha^{(i)} \exp\left(-i\alpha \sum_{j=1}^N M_{ij} \hat{\sigma}_z^{(j)}\right). \quad (12)$$

Similarly, the operator $\mathcal{U}(y)$ satisfies

$$\mathcal{U}(y)^\dagger \hat{\sigma}_j^{(i)} \mathcal{U}(y) = \sum_{\alpha \in \{-1,0,1\}} d_{j\alpha}^{(i)}(y) \hat{\sigma}_\alpha^{(i)}, \quad (13)$$

where the coefficients $d_{j\alpha}^{(i)}$ are analytical functions of the parameters y .

By definition, the expectation value $\langle \hat{\sigma}_x^{(i)} \rangle$ is given by

$$\langle \hat{\sigma}_x^{(i)} \rangle = \langle \psi(x, M) | \mathcal{U}(y)^\dagger \hat{\sigma}_x^{(i)} \mathcal{U}(y) | \psi(x, M) \rangle. \quad (14)$$

Applying Eq. (13) to the above expression, we obtain

$$\begin{aligned} \langle \hat{\sigma}_x^{(i)} \rangle &= \sum_{\alpha \in \{-1,0,1\}} d_{x\alpha}^{(i)}(y) \langle \psi(x, M) | \hat{\sigma}_\alpha^{(i)} | \psi(x, M) \rangle \\ &= \sum_{\alpha \in \{-1,0,1\}} d_{x\alpha}^{(i)}(y) \langle \psi(x) | \mathcal{V}(M)^\dagger \hat{\sigma}_\alpha^{(i)} \mathcal{V}(M) | \psi(x) \rangle. \end{aligned} \quad (15)$$

Next, we use Eq. (12) to rewrite the expectation value as

$$\begin{aligned} \langle \hat{\sigma}_x^{(i)} \rangle &= \sum_{\alpha \in \{-1,0,1\}} d_{x\alpha}^{(i)}(y) \times \\ &\times \langle \psi(x) | \hat{\sigma}_\alpha^{(i)} \exp\left(-i\alpha \sum_{j=1}^N M_{ij} \hat{\sigma}_z^{(j)}\right) | \psi(x) \rangle. \end{aligned} \quad (16)$$

Finally, we decompose the state $|\psi(x)\rangle = \otimes_{j=1}^N |\psi(x_j)\rangle$ and use it to express the expectation value as

$$\begin{aligned} \langle \hat{\sigma}_x^{(i)} \rangle &= \sum_{\alpha \in \{-1,0,1\}} d_{x\alpha}^{(i)}(y) \times \\ &\times \prod_{j=1}^N \langle \psi(x_j) | (\hat{\sigma}_\alpha^{(i)})^{\delta_{ij}} \exp\left(-i\alpha M_{ij} \hat{\sigma}_z^{(j)}\right) | \psi(x_j) \rangle. \end{aligned} \quad (17)$$

Each of the N terms in the product can now be computed analytically with a number of operations that remains independent of the total number of spins. Thus, the overall computational complexity of evaluating the expectation value in Eq. (17) scales as $\mathcal{O}(N)$.

An analogous procedure leads to similar results for the evaluation of $\langle \hat{\sigma}_z^{(i)} \hat{\sigma}_z^{(j)} \rangle$ and the gradient vectors (see Supplementary Information).

ACKNOWLEDGMENTS

We acknowledge several fruitful discussions with Alberto Mercurio, Filippo Ferrari, Luca Gravina, and Alessandro Sinibaldi. This work was supported by the Swiss National Science Foundation through Project No. 200020_215172.

CODE AND DATA AVAILABILITY

The code used to generate the results presented in this work is openly available on GitHub at <https://github.com/LorenzoFioroni/gcs-qubo-optimization>. The data that support the findings of this study are available from the corresponding author upon reasonable request.

-
- [1] B. Denton, J. Viapiano, and A. Vogl, *Health Care Management Science* **10**, 13 (2007).
- [2] B. Cardoen, E. Demeulemeester, and J. Beliën, *European Journal of Operational Research* **201**, 921 (2010).
- [3] A. R. Jordehi, *Renewable and Sustainable Energy Reviews* **103**, 308 (2019).
- [4] T. Logenthiran, D. Srinivasan, and T. Z. Shun, *IEEE Transactions on Smart Grid* **3**, 1244 (2012).
- [5] R. Z. Farahani, E. Miandoabchi, W. Y. Szeto, and H. Rashidi, *European Journal of Operational Research* **229**, 281 (2013).
- [6] V. Guihaire and J.-K. Hao, *Transportation Research Part A: Policy and Practice* **42**, 1251 (2008).
- [7] G. Kochenberger, J.-K. Hao, F. Glover, M. Lewis, Z. Lü, H. Wang, and Y. Wang, *Journal of Combinatorial Optimization* **28**, 58 (2014).
- [8] F. Barahona, *Journal of Physics A: Mathematical and General* **15**, 3241 (1982).
- [9] S. A. Vavasis, in *Encyclopedia of Optimization* (Springer US, 2001) pp. 304–307.
- [10] A. Lucas, *Frontiers in Physics* **2**, 10.3389/fphy.2014.00005 (2014).
- [11] N. Christofides, *Operations Research Forum* **3**, 20 (2022).
- [12] M. X. Goemans and D. P. Williamson, *J. ACM* **42**, 1115 (1995).
- [13] L. Bianchi, M. Dorigo, L. M. Gambardella, and W. J. Gutjahr, *Natural Computing* **8**, 239 (2009).
- [14] Z. Wang, A. Marandi, K. Wen, R. L. Byer, and Y. Yamamoto, *Physical Review A* **88**, 063853 (2013).
- [15] Y. Haribara, H. Ishikawa, S. Utsunomiya, K. Aihara, and Y. Yamamoto, *Quantum Science and Technology* **2**, 044002 (2017).
- [16] M. Calvanese Strinati and C. Conti, *Nature Communications* **13**, 7248 (2022).
- [17] S. Tsukamoto, M. Takatsu, S. Matsubara, and H. Tamura, *Sci. Tech. J* **53**, 8 (2017).
- [18] S. Qu, H. Liu, Y. Xu, L. Wang, Y. Liu, L. Zhang, J. Song, and Z. Li, *Scientific Reports* **14**, 24534 (2024).
- [19] Q.-G. Zeng, X.-P. Cui, B. Liu, Y. Wang, P. Mosharev, and M.-H. Yung, *Communications Physics* **7**,

- 10.1038/s42005-024-01705-7 (2024).
- [20] S. Kirkpatrick, C. D. Gelatt, and M. P. Vecchi, *Science* **220**, 671 (1983).
- [21] H. Goto, K. Tatsumura, and A. R. Dixon, *Science Advances* **5**, eaav2372 (2019).
- [22] N. Mohseni, P. L. McMahon, and T. Byrnes, *Nature Reviews Physics* **4**, 363 (2022).
- [23] S. Matsubara, H. Tamura, M. Takatsu, D. Yoo, B. Vatankhahghadim, H. Yamasaki, T. Miyazawa, S. Tsukamoto, Y. Watanabe, K. Takemoto, and A. Sheikholeslami, in *Complex, Intelligent, and Software Intensive Systems*, edited by L. Barolli and O. Terzo (Springer International Publishing, Cham, 2018) pp. 432–438.
- [24] S. Tsukamoto, M. Takatsu, S. Matsubara, and H. Tamura, *Fujitsu Sci. Tech. J* **53**, 8 (2017).
- [25] S. Matsubara, M. Takatsu, T. Miyazawa, T. Shibasaki, Y. Watanabe, K. Takemoto, and H. Tamura, in *2020 25th Asia and South Pacific Design Automation Conference (ASPDAC)* (2020) pp. 667–672.
- [26] A. B. Finnila, M. A. Gomez, C. Sebenik, C. Stenson, and J. D. Doll, *Chemical Physics Letters* **219**, 343 (1994).
- [27] G. E. Santoro and E. Tosatti, *Journal of Physics A: Mathematical and General* **39**, R393 (2006).
- [28] A. Das and B. K. Chakrabarti, *Reviews of Modern Physics* **80**, 1061 (2008).
- [29] T. Albash and D. A. Lidar, *Physical Review X* **8**, 031016 (2018).
- [30] E. J. Crosson and D. A. Lidar, *Nature Reviews Physics* **3**, 466 (2021).
- [31] B. Gardas, J. Dziarmaga, W. H. Zurek, and M. Zwolak, *Scientific Reports* **8**, 4539 (2018).
- [32] A. Mishra, T. Albash, and D. A. Lidar, *Nature Communications* **9**, 2917 (2018).
- [33] A. M. Childs, E. Farhi, and J. Preskill, *Physical Review A* **65**, 012322 (2001).
- [34] T. F. Rønnow, Z. Wang, J. Job, S. Boixo, S. V. Isakov, D. Wecker, J. M. Martinis, D. A. Lidar, and M. Troyer, *Science* **345**, 420 (2014).
- [35] G. E. Santoro, R. Martoňák, E. Tosatti, and R. Car, *Science* **295**, 2427 (2002).
- [36] R. Martoňák, G. E. Santoro, and E. Tosatti, *Physical Review B* **66**, 094203 (2002).
- [37] M. Hibat-Allah, E. M. Inack, R. Wiersema, R. G. Melko, and J. Carrasquilla, *Nature Machine Intelligence* **3**, 952 (2021).
- [38] G. Carleo, B. Bauer, and M. Troyer, Simulating adiabatic quantum computation with a variational approach (2024), [arXiv:2403.05147](https://arxiv.org/abs/2403.05147).
- [39] J. Bowles, A. Dauphin, P. Huembeli, J. Martinez, and A. Acín, *Physical Review Applied* **18**, 034016 (2022).
- [40] M. T. Veszeli and G. Vattay, Mean Field Approximation for solving QUBO problems (2021), [arXiv:2106.03238](https://arxiv.org/abs/2106.03238).
- [41] T. Guaita, L. Hackl, T. Shi, E. Demler, and J. I. Cirac, *Physical Review Research* **3**, 023090 (2021).
- [42] P. M. Schindler, T. Guaita, T. Shi, E. Demler, and J. I. Cirac, *Physical Review Letters* **129**, 220401 (2022).
- [43] H. M. Bauza and D. A. Lidar, Scaling Advantage in Approximate Optimization with Quantum Annealing (2024), [arXiv:2401.07184](https://arxiv.org/abs/2401.07184).
- [44] E. Farhi, J. Goldstone, S. Gutmann, and M. Sipser, Quantum Computation by Adiabatic Evolution (2000), [arXiv:quant-ph/0001106](https://arxiv.org/abs/quant-ph/0001106).
- [45] T. Albash and D. A. Lidar, *Reviews of Modern Physics* **90**, 015002 (2018).
- [46] T. Kato, *Journal of the Physical Society of Japan* **5**, 435 (1950).
- [47] C. Baldassi and R. Zecchina, *Proceedings of the National Academy of Sciences* **115**, 1457 (2018).
- [48] B. Heim, T. F. Rønnow, S. V. Isakov, and M. Troyer, *Science* **348**, 215 (2015).
- [49] S. Mandrà and H. G. Katzgraber, *Quantum Science and Technology* **3**, 04LT01 (2018).
- [50] S. Boixo, T. F. Rønnow, S. V. Isakov, Z. Wang, D. Wecker, D. A. Lidar, J. M. Martinis, and M. Troyer, *Nature Physics* **10**, 218 (2014).
- [51] T. Lanting, A. J. Przybysz, A. Yu. Smirnov, F. M. Spedalieri, M. H. Amin, A. J. Berkley, R. Harris, F. Altomare, S. Boixo, P. Bunyk, N. Dickson, C. Enderud, J. P. Hilton, E. Hoskinson, M. W. Johnson, E. Ladizinsky, N. Ladizinsky, R. Neufeld, T. Oh, I. Perminov, C. Rich, M. C. Thom, E. Tolkacheva, S. Uchaikin, A. B. Wilson, and G. Rose, *Physical Review X* **4**, 021041 (2014).
- [52] T. Albash, I. Hen, F. M. Spedalieri, and D. A. Lidar, *Physical Review A* **92**, 062328 (2015).
- [53] A. M. Perelomov, *Communications in Mathematical Physics* **26**, 222 (1972).
- [54] A. Perelomov, *Generalized Coherent States and Their Applications* (Springer, 1986).
- [55] D. P. Kingma and J. Ba, Adam: A Method for Stochastic Optimization (2017), [arXiv:1412.6980](https://arxiv.org/abs/1412.6980).
- [56] A. Montanari, *SIAM Journal on Computing* , FOCS19 (2021).
- [57] M. Dupont and B. Sundar, *Physical Review A* **109**, 012429 (2024).
- [58] Gurobi Optimization, LLC, *Gurobi Optimizer Reference Manual* (2024).

SUPPLEMENTARY INFORMATION

A. Efficient computation of the loss function

The framework we developed allows for the efficient analytical evaluation of both the expectation value of the time-dependent Hamiltonian

$$\hat{\mathcal{H}}(t) = \frac{t}{T} \hat{\mathcal{H}}_I + \left(1 - \frac{t}{T}\right) \hat{\mathcal{H}}_{\text{TF}}, \quad (18)$$

and its gradient. This is achieved by leveraging the commutation properties of the operators $\mathcal{U}(x)$ and $\mathcal{V}(M)$, as described in Guaita *et al.* [41].

First, note that the Hamiltonian consists of a sum of 1- and 2-local terms in the form of $\langle \hat{\sigma}_x^{(i)} \rangle$ and $\langle \hat{\sigma}_z^{(i)} \hat{\sigma}_z^{(j)} \rangle$, respectively. Each of these terms can be evaluated independently, allowing for the full evaluation of the loss to be carried out in parallel. In this section, we detail the procedure for estimating $\langle \hat{\sigma}_x^{(i)} \rangle$ for a given spin index i . The evaluation of $\langle \hat{\sigma}_z^{(i)} \hat{\sigma}_z^{(j)} \rangle$ follows a similar approach, which we will briefly outline at the end.

The goal is to express $\langle \hat{\sigma}_x^{(i)} \rangle$ as a linear combination of expectation values of separable operators on product states, which can be evaluated analytically with linear complexity in the number of spins. Let $\hat{\sigma}_\alpha^{(i)}$ (with a Greek index) denote the Pauli operators σ_- , σ_z and σ_+ for $\alpha \in \{-1, 0, 1\}$, respectively. The operators $\mathcal{V}(M)$ and $\mathcal{U}(y)$ obey the following relations:

$$\mathcal{V}(M)^\dagger \hat{\sigma}_\alpha^{(i)} \mathcal{V}(M) = \hat{\sigma}_\alpha^{(i)} \exp\left(-i\alpha \sum_{j=1}^N M_{ij} \hat{\sigma}_z^{(j)}\right), \quad (19)$$

$$\mathcal{U}(y)^\dagger \hat{\sigma}_j^{(i)} \mathcal{U}(y) = \sum_{k \in \{x, y, z\}} c_{jk}^{(i)}(y) \hat{\sigma}_k^{(i)}. \quad (20)$$

The coefficients $c_{jk}^{(i)}$ in Eq. (20) are analytical functions depending solely on the vector of parameters \mathbf{y}_i , and can be evaluated efficiently [41]. Next, we introduce the matrix A that transforms the Pauli basis $\{\hat{\sigma}_j^{(i)}\}_{j,i}$ to the basis $\{\hat{\sigma}_\alpha^{(i)}\}_{\alpha,i}$. Consequently, Eq. (20) can be rewritten as

$$\mathcal{U}(y)^\dagger \hat{\sigma}_j^{(i)} \mathcal{U}(y) = \sum_{\alpha \in \{-1, 0, 1\}} d_{j\alpha}^{(i)}(y) \hat{\sigma}_\alpha^{(i)}, \quad (21)$$

where $d_{j\alpha}^{(i)}(y) = \sum_{k \in \{x, y, z\}} c_{jk}^{(i)}(y) A_{k\alpha}$. Finally, we define the following states for brevity of notation

$$|\psi(x)\rangle = \mathcal{U}(x) |+\rangle^{\otimes N} \quad \text{and} \quad |\psi(x, M)\rangle = \mathcal{V}(M) \mathcal{U}(x) |+\rangle^{\otimes N}. \quad (22)$$

Using Eq. (21), the expectation value of $\hat{\sigma}_x^{(i)}$ can be expressed as

$$\langle \hat{\sigma}_x^{(i)} \rangle = \langle \psi(x, M) | \mathcal{U}(y)^\dagger \hat{\sigma}_x^{(i)} \mathcal{U}(y) | \psi(x, M) \rangle \quad (23)$$

$$= \sum_{\alpha \in \{-1, 0, 1\}} d_{x\alpha}^{(i)}(y) \langle \psi(x) | \mathcal{V}(M)^\dagger \hat{\sigma}_\alpha^{(i)} \mathcal{V}(M) | \psi(x) \rangle. \quad (24)$$

Next we apply the relation in Eq. (19), which yields

$$\langle \hat{\sigma}_x^{(i)} \rangle = \sum_{\alpha \in \{-1, 0, 1\}} d_{x\alpha}^{(i)}(y) \langle \psi(x) | \hat{\sigma}_\alpha^{(i)} \exp\left(-i\alpha \sum_{j=1}^N M_{ij} \hat{\sigma}_z^{(j)}\right) | \psi(x) \rangle. \quad (25)$$

Finally, we observe that $|\psi(x)\rangle$ is the product state

$$|\psi(x)\rangle = \mathcal{U}(x) |+\rangle^{\otimes N} = \bigotimes_{j=1}^N \exp(-i\mathbf{x}_j \cdot \boldsymbol{\sigma}^{(j)}) |+\rangle = \bigotimes_{j=1}^N |\psi(x_j)\rangle. \quad (26)$$

Employing the relation in Eq. (26), the expectation value is rewritten as a factorized product of single-spin expectation values, and can therefore be evaluated efficiently in time $\mathcal{O}(N)$:

$$\langle \hat{\sigma}_x^{(i)} \rangle = \sum_{\alpha \in \{-1,0,1\}} d_{x\alpha}^{(i)}(y) \prod_{j=1}^N \langle \psi(x_j) | (\hat{\sigma}_\alpha^{(i)})^{\delta_{ij}} \exp(-i\alpha M_{ij} \hat{\sigma}_z^{(j)}) | \psi(x_j) \rangle. \quad (27)$$

A similar procedure can be followed to evaluate the expectation value of 2-local operators $\langle \hat{\sigma}_z^{(i)} \hat{\sigma}_z^{(j)} \rangle$. We now use, in addition to Eq. (20), the unitary relation $\mathcal{U}(x)\mathcal{U}(x)^\dagger = \mathbb{I}$ to get

$$\langle \hat{\sigma}_z^{(i)} \hat{\sigma}_z^{(j)} \rangle = \langle \psi(x, M) | \mathcal{U}(y)^\dagger \hat{\sigma}_z^{(i)} \hat{\sigma}_z^{(j)} \mathcal{U}(y) | \psi(x, M) \rangle \quad (28)$$

$$= \langle \psi(x, M) | \mathcal{U}(y)^\dagger \hat{\sigma}_z^{(i)} \mathcal{U}(y) \mathcal{U}(y)^\dagger \hat{\sigma}_z^{(j)} \mathcal{U}(y) | \psi(x, M) \rangle \quad (29)$$

$$= \sum_{\alpha, \beta \in \{-1,0,1\}} d_{z\alpha}^{(i)}(y) d_{z\beta}^{(j)}(y) \langle \psi(x) | \mathcal{V}(M)^\dagger \hat{\sigma}_\alpha^{(i)} \hat{\sigma}_\beta^{(j)} \mathcal{V}(M) | \psi(x) \rangle. \quad (30)$$

Similarly, we employ Eq. (19) as well as $\mathcal{V}(M)\mathcal{V}(M)^\dagger = \mathbb{I}$ to obtain

$$\langle \hat{\sigma}_z^{(i)} \hat{\sigma}_z^{(j)} \rangle = \sum_{\alpha, \beta \in \{-1,0,1\}} d_{z\alpha}^{(i)}(y) d_{z\beta}^{(j)}(y) \langle \psi(x) | \hat{\sigma}_\alpha^{(i)} \exp\left(-i\alpha \sum_{k=1}^N M_{ik} \hat{\sigma}_z^{(k)}\right) \hat{\sigma}_\beta^{(j)} \exp\left(-i\beta \sum_{k=1}^N M_{jk} \hat{\sigma}_z^{(k)}\right) | \psi(x) \rangle \quad (31)$$

$$= \sum_{\alpha, \beta \in \{-1,0,1\}} d_{z\alpha}^{(i)}(y) d_{z\beta}^{(j)}(y) \prod_{k=1}^N \langle \psi(x_k) | (\hat{\sigma}_\alpha^{(i)})^{\delta_{ik}} \exp\left(-i\alpha M_{ik} \hat{\sigma}_z^{(k)}\right) (\hat{\sigma}_\beta^{(j)})^{\delta_{jk}} \exp\left(-i\beta M_{jk} \hat{\sigma}_z^{(k)}\right) | \psi(x_k) \rangle, \quad (32)$$

where we used the factorized expression for $|\psi(x)\rangle$ in the second step. Note that, although the sums now run over nine possible combinations of α and β , the scaling of the computation with respect to the number of spins remains linear.

B. Efficient computation of the gradient vector

A procedure akin to the one outlined in the previous section allows for the efficient computation of the gradient of the loss function with respect to the variational parameters. Analogously to our previous discussion, we focus on the expectation value $\langle \hat{\sigma}_x^{(i)} \rangle$ of a local operator and show that its gradient vector can be evaluated analytically with an $\mathcal{O}(N)$ complexity. A similar result can be equivalently proven for $\langle \hat{\sigma}_z^{(i)} \hat{\sigma}_z^{(j)} \rangle$.

Let us denote with P_{ij}^α the j -th element of the product in Eq. (27)

$$P_{ij}^\alpha(x, M) = \langle \psi(x_j) | (\hat{\sigma}_\alpha^{(i)})^{\delta_{ij}} \exp(-i\alpha M_{ij} \hat{\sigma}_z^{(j)}) | \psi(x_j) \rangle. \quad (33)$$

The expectation value in Eq. (27) can thus be written as

$$\langle \hat{\sigma}_x^{(i)} \rangle = \sum_{\alpha \in \{-1,0,1\}} d_{x\alpha}^{(i)}(y) P_i^\alpha(x, M), \quad (34)$$

where we defined $P_i^\alpha(x, M) = \prod_j P_{ij}^\alpha(x, M)$. Note that the evaluation of $P_i^\alpha(x, M)$ is efficient and can be carried out with $\mathcal{O}(1)$ complexity.

We first discuss the computation of the gradient with respect to the x parameters. The only dependence of $\langle \hat{\sigma}_x^{(i)} \rangle$ on the parameter x_{lm} is through the single-spin state $|\psi(x_l)\rangle$ which, in turn, only appears in P_{il}^α . Consequently, the derivative of $\langle \hat{\sigma}_x^{(i)} \rangle$ with respect to x_{lm} can be written as

$$\frac{\partial \langle \hat{\sigma}_x^{(i)} \rangle}{\partial x_{lm}} = \sum_{\alpha \in \{-1,0,1\}} d_{x\alpha}^{(i)}(y) \frac{\partial P_{il}^\alpha}{\partial x_{lm}} \prod_{j \neq l} P_{ij}^\alpha = \sum_{\alpha \in \{-1,0,1\}} d_{x\alpha}^{(i)}(y) \frac{P_i^\alpha}{P_{il}^\alpha} \frac{\partial P_{il}^\alpha}{\partial x_{lm}} \quad (35)$$

Let us now define the derived state

$$|\partial_{x_{lm}} \psi(x_l)\rangle = \frac{\partial |\psi(x_l)\rangle}{\partial x_{lm}} = \frac{\partial}{\partial x_{lm}} \exp\left(-i \sum_{k \in \{x,y,z\}} x_{lk} \hat{\sigma}_k^{(l)}\right) |+\rangle = -i \hat{\sigma}_m^{(l)} |\psi(x_l)\rangle. \quad (36)$$

We can finally express the derivative $\partial P_{il}^\alpha / x_{lm}$ as

$$\frac{\partial P_{il}^\alpha}{\partial x_{lm}} = \langle \partial_{x_{lm}} \psi(x_l) | (\hat{\sigma}_\alpha^{(i)})^{\delta_{il}} \exp\left(-i\alpha M_{il} \hat{\sigma}_z^{(l)}\right) | \psi(x_l) \rangle + \langle \psi(x_l) | (\hat{\sigma}_\alpha^{(i)})^{\delta_{il}} \exp\left(-i\alpha M_{il} \hat{\sigma}_z^{(l)}\right) | \partial_{x_{lm}} \psi(x_l) \rangle. \quad (37)$$

Notice that Eq. (37), and therefore the derivative $\partial \langle \hat{\sigma}_x^{(i)} \rangle / \partial x_{lm}$ can be evaluated with $\mathcal{O}(1)$ complexity. Thus, the computation of the full gradient vector with respect to the x parameters $\nabla_x \langle \hat{\sigma}_x^{(i)} \rangle$ has a linear cost in the number of spins.

Following a similar procedure, we observe that $\langle \hat{\sigma}_x^{(i)} \rangle$ depends on the parameter M_{lm} only if $l = i$. We thus restrict to this case and obtain

$$\frac{\partial \langle \hat{\sigma}_x^{(i)} \rangle}{\partial M_{im}} = \sum_{\alpha \in \{-1,0,1\}} d_{x\alpha}^{(i)}(y) \frac{\partial P_{im}^\alpha}{\partial M_{im}} \prod_{j \neq i} P_{ij}^\alpha = \sum_{\alpha \in \{-1,0,1\}} d_{x\alpha}^{(i)}(y) \frac{P_i^\alpha}{P_{ii}^\alpha} \frac{\partial P_{im}^\alpha}{\partial M_{im}}, \quad (38)$$

where $\partial P_{im}^\alpha / \partial M_{im}$ is found to be

$$\frac{\partial P_{im}^\alpha}{\partial M_{im}} = -i\alpha \langle \psi(x_m) | (\hat{\sigma}_\alpha^{(i)})^{\delta_{im}} \hat{\sigma}_z^{(m)} \exp\left(-i\alpha M_{im} \hat{\sigma}_z^{(m)}\right) | \psi(x_m) \rangle. \quad (39)$$

Also in this case the computation of each derivative has constant cost in the number of spins. Since the only parameters that can yield a non-zero derivative are $\{M_{im}\}_{m=1}^N$, the computation of the full gradient vector $\nabla_M \langle \hat{\sigma}_x^{(i)} \rangle$ has $\mathcal{O}(N)$ complexity.

Finally, we turn our focus to the y parameters. As previously mentioned, the coefficients $d_{x\alpha}^{(i)}(y)$ only depend on the y_i vector of parameters. Consequently, we anticipate $\partial \langle \hat{\sigma}_x^{(i)} \rangle / \partial y_{lm} = 0$ for $l \neq i$. We can therefore compute the derivative of $\langle \hat{\sigma}_x^{(i)} \rangle$ with respect to the parameter y_{im} , finding

$$\frac{\partial \langle \hat{\sigma}_x^{(i)} \rangle}{\partial y_{im}} = \sum_{\alpha \in \{-1,0,1\}} \frac{\partial d_{x\alpha}^{(i)}(y)}{\partial y_{im}} \prod_{j=1}^N P_{ij}^\alpha(x, M). \quad (40)$$

The derivatives $\partial d_{x\alpha}^{(i)}(y) / \partial y_{im}$ are analytical functions of the y parameters, similar to $d_{x\alpha}^{(i)}(y)$. The expression in Eq. (40) can be evaluated with $\mathcal{O}(N)$ complexity. Since $\{y_{im}\}_{m=1}^3$ are the only parameters that can yield a non-zero derivative, the complexity for the computation of the full gradient vector remains unchanged and scales linearly with the number of spins.